

Minerals and ore deposits exploration using meta-heuristic based optimization on magnetic data

Mohamed GOBASHY¹ , Maha ABDELAZEEM^{2,*} ,
Mohamed ABDRABOU¹

¹ Cairo University, Faculty of Science, Geophysics Department, Giza, Egypt

²National Research Institute of Astronomy and Geophysics (NRIAG), Helwan, Cairo, Egypt

Abstract: The difficulties in unravelling the tectonic structures, in some cases, prevent the understanding of the ore bodies' geometry, leading to mistakes in mineral exploration, mine planning, evaluation of ore deposits, and even mineral exploitation. For that reason, many geophysical techniques are introduced to reveal the type, dimension, and geometry of these structures. Among them, electric methods, self-potential, electromagnetic, magnetic and gravity methods. Global meta-heuristic technique using Whale Optimization Algorithm (WOA) has been utilized for assessing model parameters from magnetic anomalies due to a thin dike, a dipping dike, and a vertical fault like/shear zone geological structure. These structures are commonly associated with mineralization. This modern algorithm was firstly applied on a free-noise synthetic data and to a noisy data with three different levels of random noise to simulate natural and artificial anomaly disturbances. Good results obtained through the inversion of such synthetic examples prove the validity and applicability of our algorithm. Thereafter, the method is applied to real case studies taken from different ore mineralization resembling different geologic conditions. Data are taken from Canada, United States, Sweden, Peru, India, and Australia. The obtained results revealed good correlation with previous interpretations of these real field examples.

Key words: magnetic anomaly, ore deposits, whale algorithm, artificial intelligence, inversion, mineralization

1. Introduction

Magnetic prospecting method has been used to investigate a broad diversity of geological structures varying in size and depth from shallow ore bodies to deep basement structures. For detecting areas of large thickness of high potentially oil-bearing sedimentary rocks in oil exploration and, for mapping

*corresponding author: e-mail: maazeem03@hotmail.com

and outlining ore deposits (e.g., iron, and copper) in ore prospecting, magnetic survey is still in use as a powerful geophysical technique in tracking mineralized zones. The general target of the magnetic surveys is, consequently, to investigate minerals or rocks having contrast in the magnetic properties (i.e., magnetic susceptibility) with the surroundings to discover them as anomalies in the magnetic field intensity of the earth. Occasionally, a single magnetic anomaly can be isolated from the regional trend and dealt with as an individual magnetized source. However, in such cases, the interpretation of magnetic data is normally exposed to ambiguity. Variant geometric shapes below can give similar magnetic response at the earth's surface. A single solution, although, can be obtained immediately from magnetic data if the shape of the buried body is known and a constant contrast in the magnetic susceptibility is present. This point was numerically confirmed through numerous researchers by categorizing nearly all of the magnetic source bodies in exploration studies into four simple stationary shapes: the horizontal cylinder, the sphere, the geologic contact and the thin sheet (*Nettleton, 1976; Abdelazeem, 2001; Li, 2003*). These simple geologic sources are frequently acceptable approximations to familiar geologic bodies included in the process of interpretation of magnetic field data quantitatively.

For these kinds of structures, numerous methods have been developed and utilized for explanation of magnetic field anomalies resulted from simple shaped bodies aiming to estimate the depth to the subsurface body, location of body, the amplitude coefficient, and the index parameter from magnetic anomalies. Among these techniques for example are: monograms (*Prakasa Rao et al., 1986*), theoretical matching standard curves (*Gay, 1963, 1965; Atchuta Rao and Ram Babu, 1983*), characteristic curves methods (*Bruckshaw and Kunaratnam, 1963; Grant and West, 1965; Koulomzine et al., 1970; Telford et al., 1976; Rao and Murthy, 1978*), correlation factors between successive least-squares residual anomalies (*Abdelrahman et al., 1989*), Hilbert transforms (*Mohan et al., 1982*), Euler deconvolution approach (*Reid et al., 1990; Gerovska and Araúz-Bravo, 2003; Salem and Ravat, 2003; Pasteka, 2006*) analytic signal derivatives (*Salem, 2005*), Werner deconvolution approach (*Hartman et al., 1971; and Ku and Sharp, 1983*), and fair function minimization (*Tlas and Asfahani, 2011*). Global optimization techniques like very fast simulated annealing (VFSA), simulated

annealing, higher-order horizontal derivative methods and particle swarm optimization (PSO) (*Sweilam et al., 2007, 2008; Göktürkler and Balkaya, 2012; Biswas and Sharma, 2014a,b; Biswas, 2015; Biswas and Acharya, 2016; Ekinçi, 2016; Singh and Biswas, 2016*) have been successfully used to obtain model parameters from nonlinear inversion problems.

Though, mainly, the assessment of model unknowns, namely amplitude coefficient, depth, dip angle of the dike and effective magnetization angle of the subsurface model (e.g. thin dike, dipping dike and vertical fault), is achieved by inversion approaches as referred above. Consequently, the precision of the outcomes acquired by the above- referred techniques depends on the accuracy by which the anomaly can be isolated from the measured magnetic anomaly.

Whale Optimization Algorithm (WOA) has been recently used in solving the ill-posed inverse problem in geophysics. WOA inversion has been utilized to invert Self-Potential anomalies due to 2D inclined sheet and simple geometric bodies like (sphere, vertical cylinder, and horizontal cylinder) (*Gobashy et al., 2020; Abdelazeem et al., 2019*).

In this work, a rapid and effective modeling technique based on the Whale Optimization Algorithm (WOA) global meta-heuristic algorithm (*Mirjalili and Lewis, 2016*) was applied for inverting the highly ill-posed magnetic field due to thin dike, dipping dike and vertical fault. For a thin dike model, this method was applied to solve for four parameters, namely the depth (h), effective magnetization intensity (A_e), horizontal location (x_0), and effective magnetization inclination of the dike (θ); for a dipping dike model, it was applied to extract five unknowns, namely the depth (h), half-width (b), intensity of magnetization (I), inclination of the magnetic vector (ψ), and dip angle of the dike (θ), and for a vertical fault it was applied to estimate five unknowns, namely the effective magnetization intensity (K), horizontal location (x_0), effective magnetization inclination (θ), depth to the upper edge (z), and depth to the lower edge of the fault (z_b).

The accuracy of this meta-heuristic optimization algorithm is practically examined via synthetic examples, using simulated data created from three models (i.e. thin dike, dipping dike, and vertical fault) with three different levels of random noise. As it is theoretically proved, the suggested algorithm is afterwards applied to real magnetic profiles over mineralized zones resembling different geologic structures and geometries taken from Canada,

United States, Sweden, Peru, India, and Australia. There is an excellent correlation between the outcomes attained from the suggested algorithm and those obtained by other techniques.

2. Methodology

2.1. Magnetic problem formulation

2.1.1. Thin dike-like structure

For a magnetic effect $F(x)$ generated by a thin dike model of infinite depth extent (Fig. 1) that may be either in total, vertical, or horizontal magnetic components, the general formula is given by (Gay, 1963) as:

$$F(x) = A_e \frac{h \cos \theta + (x - x_0) \sin \theta}{(x - x_0)^2 + h^2}, \tag{1}$$

where $A_e = K \cdot h$, and K refers to the effective magnetization intensity or the amplitude coefficient, h defines the depth to the top of the buried thin

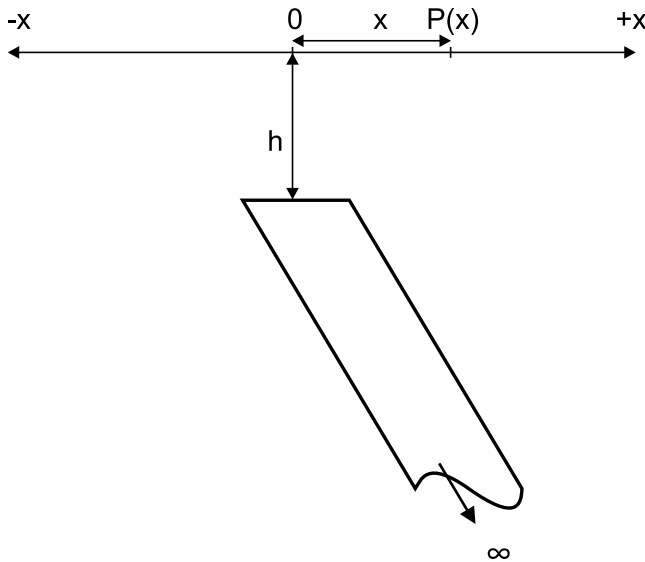


Fig. 1. Cross-sectional view of a two-dimensional thin dike model (Tlas and Asfahani, 2011).

dike-like structure, x is the horizontal coordinate along the profile, θ refers to the index parameter or the effective magnetization angle, and x_0 defines the true origin of the observed magnetic anomaly.

2.1.2. Dipping dike-like structure

The vertical magnetic anomaly $V(x)$ generated from an infinitely dipping dike model with a uniform magnetization (Fig. 2) is expressed by (*Grant and West, 1965*) as:

$$V(x) = 2I \sin \theta \left[\cos \psi \left(\tan^{-1} \frac{x+b}{h} - \tan^{-1} \frac{x-b}{h} \right) + \frac{1}{2} \sin \psi \left(\ln \frac{h^2 + (x+b)^2}{h^2 + (x-b)^2} \right) \right], \tag{2}$$

where $I = k \cdot F_e$, I is the intensity of magnetization (nT), k refers to the magnetic susceptibility contrast, F_e is the vertical component of the local ambient field (nT), b is the half width of the dike (m), h defines depth of the upper surface (m), θ refers to the dip angle of the dike (degree), and ψ is the inclination of the magnetization vector (degree).

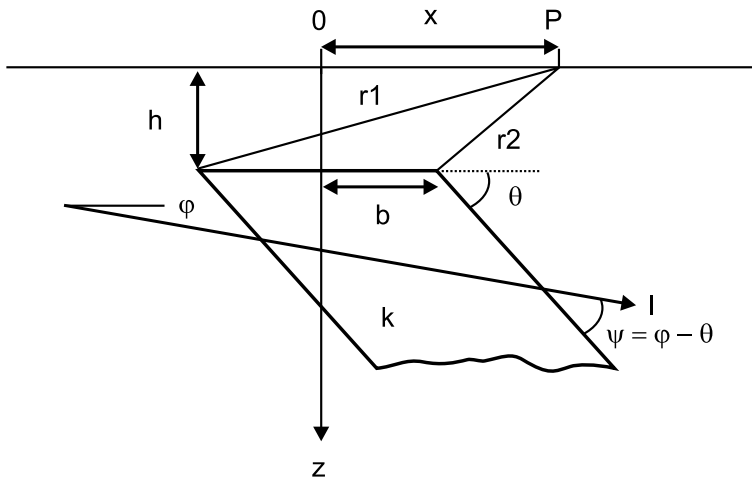


Fig. 2. Geometry of a thick dipping dike model.

2.1.3. Vertical fault model

The magnetic effect $F(x)$ of a two-dimensional magnetized fault model that could be in total, horizontal or vertical field at a discrete point x_i along the horizontal coordinate (x) (Fig. 3) is expressed by the following equation (Atchuta Rao and Ram Babu, 1983, and Tlas and Asfahani, 2011) as:

$$\begin{aligned}
 F(x) = k \frac{z}{z_b - z} & \left[\cos \theta \left(\ln \left| \sin \left(\tan^{-1} \frac{x_i - x_0}{z} \right) \right| - \right. \right. \\
 & \left. \left. - \ln \left| \sin \left(\tan^{-1} \frac{x_i - x_0}{z_b} \right) \right| \right) \right] + \\
 & \left. + \sin \theta \left(\tan^{-1} \frac{x_i - x_0}{z} - \tan^{-1} \frac{x_i - x_0}{z_b} \right) \right], \tag{3} \\
 & (i = 1, 2, 3, \dots, N)
 \end{aligned}$$

where θ refers to the effective magnetization inclination or (the index parameter), k is the effective magnetization intensity or (the amplitude coefficient), z is the depth to the upper edge of the fault directly underneath the horizontal position (x_0) of the edge of the fault, x_i is an individual point through the horizontal coordinate location (x) where the measured magnetic anomaly is located, and z_b defines the depth to the lower edge of the fault as shown in (Fig. 3).

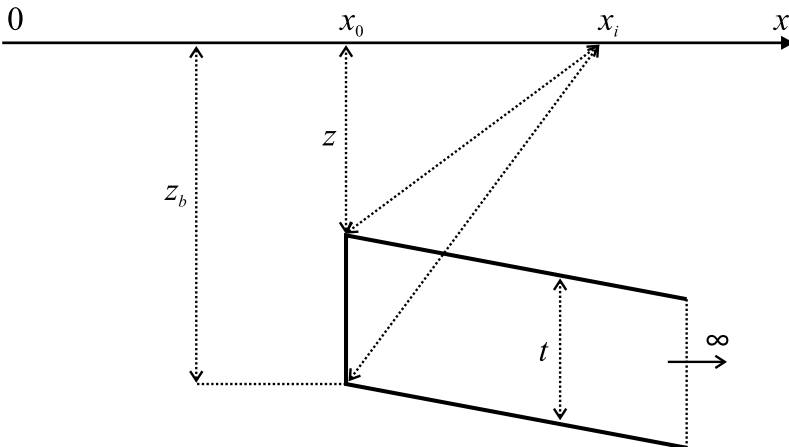


Fig. 3. Cross-sectional view of a two-dimensional vertical fault model (Tlas and Asfahani, 2011).

2.2. Inversion

Several global optimization techniques have been evolved in the past decades based upon various important concepts as mentioned above. The principal goal of geophysical inversion is to optimize a cost function or an objective function in the modeling of geophysical data. Numerous optimization approaches like genetic algorithms (GA), very fast simulated annealing (VFSA), particle swarm optimization (PSO), artificial neural networks (ANN), differential evolution (DE), black hole algorithm (BHA) and Simplex algorithm (*Abdelazeem and Gobashy, 2006; Biswas and Sharma, 2015, 2016; Monteiro Santos, 2010; El-Kaliouby and Al-Garni, 2009; Li and Yin, 2012; Sungkono and Desa Warnana, 2018; Abdelrahman et al., 2019*) were successfully utilized to minimize an objective function of observed geophysical data to find model parameters (i.e. various geophysical information).

Whale Optimization Algorithm (WOA) is a recent optimization algorithm which was first proposed by (*Mirjalili and Lewis, 2016*). WOA was inspired from nature that imitates the humpback whale behavior. Unlike genetic algorithm (GA) and particle swarm optimization (PSO), the WOA is very fast, simple in its concept, reliable, does not need adjusting or tuning its parameters, and unlike modular neural network (MNN) technique (*El-Kaliouby and Al-Garni, 2009*), it does not require training which it takes longer time and represents an important step in neural network.

Briefly, WOA implements the following strategies used by the humpback whales such as bubble-net attacking and searching for the prey.

1. Bubble-net attacking:

When two or more whales swim in a shrinking ring or circle, bubbles are created to encircle the prey along a spiral path. Some search agents (whales) are pushing the prey to the surface while the others lead the prey to the net. The positions of the search agents are updated according to the position of the best search agent. In a mathematical form, this mechanism of encircling the prey can be expressed as follows (*Abdel-Basset et al., 2018*):

$$D = |C \cdot \omega^* - x^t|, \quad (4)$$

$$x^{t+1} = \omega^* - A \cdot D, \quad (5)$$

$$A = 2a \cdot r - a, \quad (6)$$

$$C = 2 \cdot r, \quad (7)$$

where, D is the distance between the current search agent x^t and the best search agent ω^* so far at t iteration. A and C are coefficient vectors, A is a random value in the range $[-a, a]$, x^t is the position vector, $||$ is the absolute value, and \cdot is an element-by-element multiplication. It is worth mentioning here that ω^* should be updated in each iteration if there is a better solution. r is a random number in $[0, 1]$. a is linearly decreased from 2 to 0 over the course of iterations (in both exploration and exploitation phases).

The value of A decreases from 2 to 0 during iterations and C is a coefficient. Different places around the best agent can be achieved with respect to the current position by adjusting the value of A and C vectors. The spiral shaped path's behavior can be given as (*Abdel-Basset et al., 2018*):

$$x^{t+1} = D' \cdot e^{bi} \cdot \cos(2\pi l) + \omega^*, \quad (8)$$

$$D' = |\omega^* - x^t|, \quad (9)$$

where, D' is the absolute value for the distance between x^t and ω^* . b defines the shape of the logarithmic spiral, l is a random value $\in [-1, 1]$. WOA implements the two behaviors of bubble-net attacking encircling: the prey circle and the spiral movement with equal probabilities as follows:

$$x^{t+1} = \begin{cases} \omega^* - A \cdot D & p < 0.5, \\ D' \cdot e^{bi} \cdot \cos(2\pi l) + \omega^* & p \geq 0.5. \end{cases} \quad (10)$$

2. Searching for the prey:

WOA makes a tradeoff between the exploration, which can be done by selecting a random search agent x_{rand} , and the exploitation, which is done by selecting the best search agent:

$$D = |C \cdot x_{rand} - x^t|, \quad (11)$$

$$x^{t+1} = x_{rand} - A \cdot D. \quad (12)$$

A detailed explanation and more discussion of the stability of WOA can be found in *Mirjalili and Lewis (2016)*; *Abdel-Basset et al. (2018)*; *Gobashy et al. (2020)*; *Abdelazeem et al. (2019)*. Fig. 4a shows a flowchart for the WOA heuristic algorithm, Fig. 4b shows the Bubble-net search mechanism,

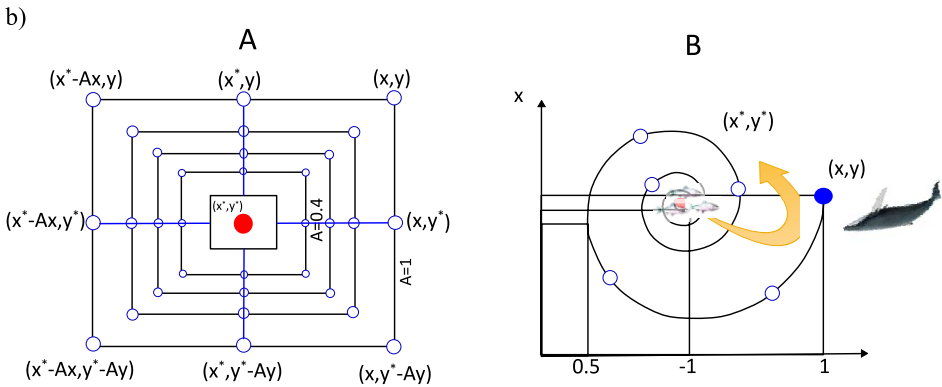
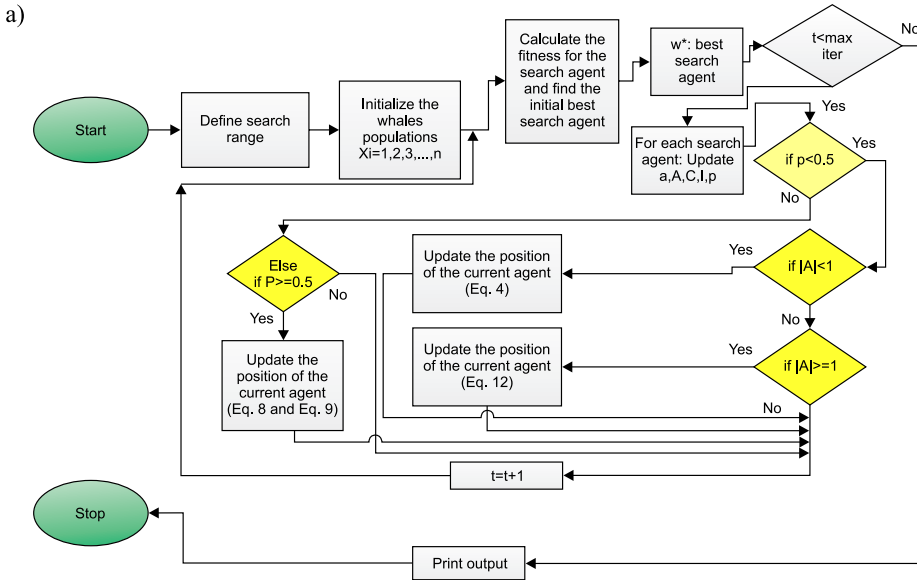


Fig. 4. a) A flowchart for the WOA heuristic algorithm, b) Bubble-net search mechanism (x^* is the best solution obtained so far): (A) Shrinking encircling mechanism and (B) spiral updating position (modified after *Abdel-Basset et al., 2018*).

where x^* is the best solution obtained so far and x , is the initial solution. Left panel is the shrinking encircling mechanism and right panel is spiral updating position (modified after *Abdel-Basset et al., 2018*).

The magnetic data in this paper were inverted using the misfit function (φ) given in Eq. (13), *Sharma and Biswas (2013)*. The misfit error between the measured and inverted magnetic data was evaluated utilizing the average relative error in percentage that was given by Eq. (14):

$$\varphi = \frac{1}{N} \sum_{i=1}^N \left(\frac{M_i^0 - M_i^c}{|M_i^0| + (M_{max}^0 - M_{min}^0)/2} \right)^2, \quad (13)$$

$$Misfit\ Error(\%) = \left(\frac{100}{N} \right) \sqrt{\sum_{i=1}^N \left[\frac{M_i^0 - M_i^c}{M_i^0} \right]^2}, \quad (14)$$

where, N is the number of the measured magnetic readings, M_{min}^0 and M_{max}^0 are the minimum and maximum values, respectively, of the observed data, M_i^0 and M_i^c are the observed magnetic data and calculated one, respectively. In minimizing the ill-posed magnetic inverse problem utilizing the above expression, WOA was observed to be highly stable in the inversion process. A flowchart for the complete process of WOA is given in Fig. 4.

3. Theoretical examples

To check the above formulation, the WOA optimization algorithm was used for the optimization of Eq. (4) for synthetic magnetic data generated via three different models (thin dike, dipping dike, and vertical fault). Every theoretical model is tested with and without random error, and the highest random error added is 30%. The WOA inversion was executed utilizing two hundreds search agents and three hundreds iterations.

3.1. Thin dike model

Theoretical data were created for a thin dike model utilizing Eq. (1) with $A_e = 1000$ nT.m, $x_0 = 5$ m, $h = 8$ m, $\theta = -40^\circ$. The number of points in this synthetic case is 61 data points with 1 meter separating between

each two successive points. Table 1 depicts the correct model parameters, search spaces for every parameter and the inverted model parameters after inversion process. For noise free data, the misfit error between observed and inverted data is 0.0214%. In Fig. 5a, the inverted magnetic data and synthetic one are depicted together. The convergence of the cost function with iteration number is presented in Fig. 5b. Residuals between synthetic magnetic data and inverted response are displayed in Fig. 5c. The suggested algorithm is additionally tested on a contaminated data with three different noise levels (10%, 20%, and 30%). The highest error observed is 1.1628% at 30% random noise.

Table 1. True and inverted model parameters using WOA algorithm due to a thin dike model. The search spaces for WOA are: 600 : 1500 nT.m (A), $-3 : 10$ m (x_0), $-70 : -30^\circ$ (θ), and 4 : 12 m (h).

Parameter	A_e (nT.m)	x_o (m)	θ ($^\circ$)	h (m)	Misfit error (%)
true model	1000	5	-40	8	–
noise free	999.977	4.999	-40.009	8.006	0.0214
10% noise	989.813	5.024	-39.981	7.946	0.4019
20% noise	1008.087	4.972	-40.431	8.272	1.0086
30% noise	1003.015	4.848	-39.212	7.992	1.1628

In the process of optimization of Eq. (4), each unknown parameter is constrained with lower and upper bounds according to the true values of these parameters, but in real field examples these bounds are controlled with the present geologic conditions in the study area. The inverted data and noisy ones of the three added levels of noise 10%, 20% and 30% are depicted in Fig. 6a,b and c, respectively. There is a good agreement between the correct model parameters and inverted solutions via WOA.

3.2. Dipping dike model

Alike the above theoretical example of the thin dike model, the true model parameters, the search spaces of the model parameters used during the inversion, and the estimated ones of a dipping dike model are given in Table 2. The dipping dike parameters are $b = 1$ m, $I = 100$ nT, $\theta = 50^\circ$, $h = 10$ m, $\psi = 30^\circ$ which were used to generate the synthetic data using

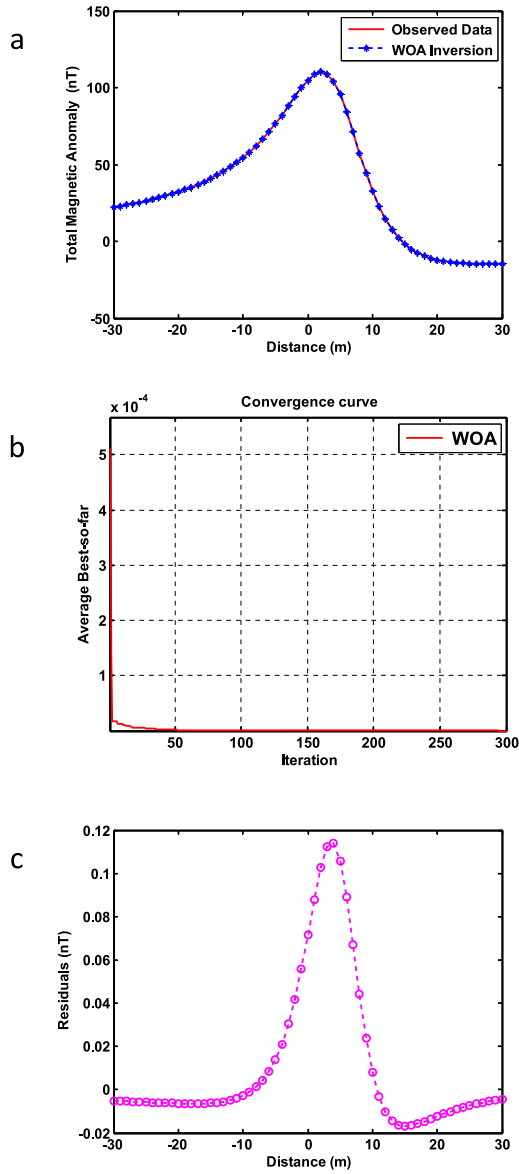


Fig. 5. WOA inversion results for synthetic magnetic anomaly of a noise free 2-D thin dike model. a) comparison between inverted response (blue) and synthetic data (red), b) convergence curve of the objective function with WOA iterations values, and c) residuals between synthetic magnetic data and inverted magnetic data from WOA.

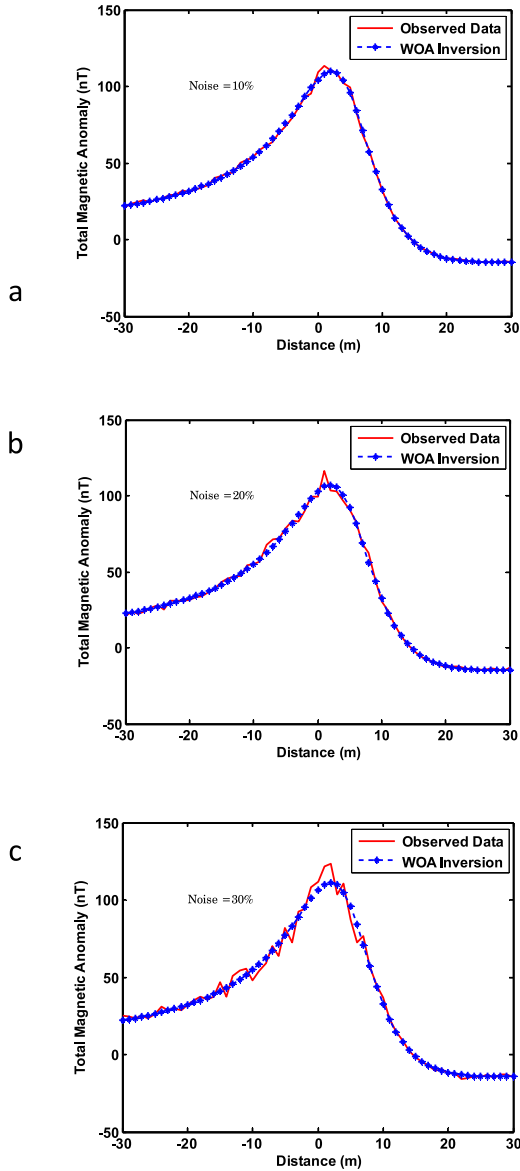


Fig. 6. Synthetic magnetic anomaly of 2-D thin dike model with their WOA inversion responses for a) with 10 % of random noise, b) with 20 % of random noise and c) with 30% of random noise.

Table 2. True and inverted model parameters using WOA algorithm due to a dipping dike model. The search spaces for WOA are: 5 : 15 m (h), 0.7 : 1.5 m (b), 80 : 120 nT (I), 40 : 60° (θ), and 20 : 40° (ψ).

Parameter	h (m)	b (m)	I (nT)	θ (°)	ψ (°)	Misfit error (%)
true model	10	1	100	50	30	–
noise free	10	1.002	97.168	51.835	30	0.0029
10% noise	10.045	0.980	104.448	48.496	30.096	0.2478
20% noise	10.127	1.168	97.723	41.999	30.158	0.6793
30% noise	10.031	1.035	89.261	55.900	29.909	0.8374

Eq. (2). The misfit error between observed and inverted data is 0.0029% for free noise case. Fig. 7a shows the synthetic magnetic data and the inverted one as resulted from WOA inversion. The behavior of the cost function is depicted in Fig. 7b. Differences between the synthetic magnetic data and computed one are displayed in Fig. 7c. The inversion of 30% noise, added to the synthetic data, produces a misfit error registered less than 0.9%. The computed magnetic data and synthetic noisy ones for (10%, 20% and 30%) are shown in Fig. 8a,b and c, respectively. There is a good correlation between the exact model parameters and the solutions obtained via WOA.

3.3. Vertical fault model

Table 3 contains the exact model parameters, the parameter spaces utilized in the WOA inversion and the calculated parameters. The vertical fault parameters used to create the theoretical magnetic data are $z = 10$ km,

Table 3. True and inverted model parameters using WOA algorithm due to a vertical fault model. The search spaces for WOA are: 1 : 15 km (z), 20 : 30 km (z_b), 0.1 : 0.9 km (x_0), $-90 : 90^\circ$ (θ), and 50 : 150 nT (K).

Parameter	z (km)	z_b (km)	x_0 (km)	θ (°)	K (nT)	Misfit error (%)
true model	10	25	0.5	30	100	–
noise free	9.843	25.741	0.266	30.502	102.568	0.0723
5% noise	9.449	26.142	0.349	30.248	106.538	0.1609
10% noise	10.637	24.394	0.328	30.459	93.987	0.3321
15% noise	10.612	24.999	0.159	30.571	94.702	0.4344

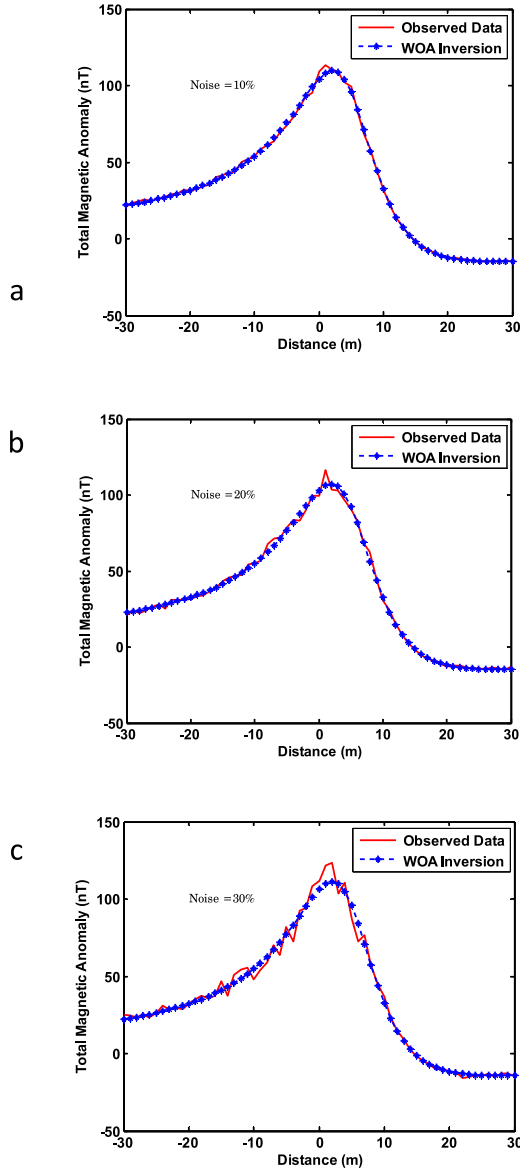


Fig. 7. WOA inversion results for synthetic magnetic anomaly of a noise free 2-D dipping dike model. a) comparison between inverted response (blue) and synthetic data (red), b) convergence curve of the objective function with WOA iterations values, and c) residuals between synthetic magnetic data and inverted magnetic data from WOA.

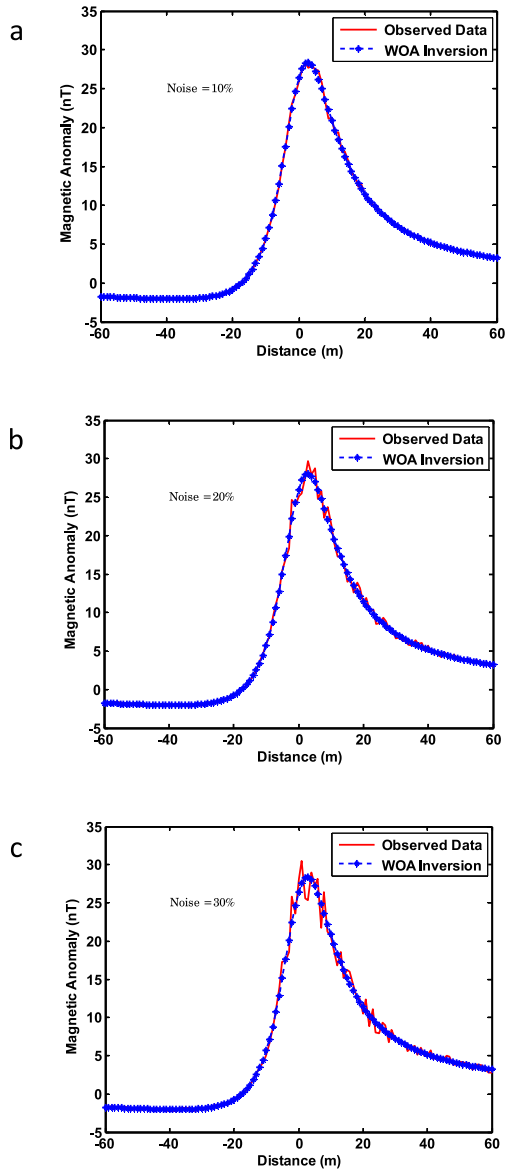


Fig. 8. Synthetic magnetic anomaly of 2-D dipping dike model with their WOA inversion responses for a) with 10% of random noise, b) with 20% of random noise and c) with 30% of random noise.

$x_0 = 0.5$ km, $z_b = 25$ km, $k = 100$ nT, $\theta = 30^\circ$ using Eq. (3). Inversion of noise free synthetic data, concludes a misfit error not more than 0.0723% between synthetic and inverted response. A comparison between the synthetic magnetic data and calculated one via WOA is given in Fig. 9a. Average best of the misfit function is depicted in Fig. 9b, while Fig. 9c displays the differences between theoretical and computed magnetic data. The highest misfit error observed is 0.1609%, 0.3321%, and 0.4344% for the inverted 5%, 10%, and 15% noisy data as given in Table 3. The computed magnetic data and synthetic noisy one for 5%, 10%, and 15% random error are displayed together in Fig. 10a,b and c, respectively. It can be observed that the estimated parameters from the WOA inversion of data with noise are in excellent agreement with the exact ones.

4. Real examples

Real magnetic field data from variant locations over the world were studied to test the power and stability of the WOA inversion.

4.1. Diabase dike, Pishabo Lake magnetic anomaly, Ontario, Canada

This anomaly represents a total field magnetic example which was measured over an outcrop of a gabbroic olivine diabase dike, Pishabo Lake, Ontario, Canada (*McGrath and Hood, 1970; Al-Garni, 2017*) and is depicted in Fig. 11a. Aeromagnetic data has been recorded at 304m elevation. The width of this dike is around 220 m. The entire length of the profile is 2000 m and 40 m sampling interval was used in the digitizing of this profile, so 51 data points used in the inversion. The geological cross-section of this magnetic profile is shown in Fig. 11b (after *McGrath and Hood, 1970*). The inverted parameters by WOA are as follows: $A_e = 144200.88$ nT.m, $x_0 = -6.41$ m, $h = 339.29$ m, $\theta = -37.14^\circ$. The inverted outcomes by WOA suggest that those findings agree well with those obtained by (*El-Araby, 2003; Ekinci, 2016; Al-Garni, 2017*) as given in Table 4. The misfit error between observed and inverted data is 2.7051%. The average best of the cost function is displayed in Fig. 11c.

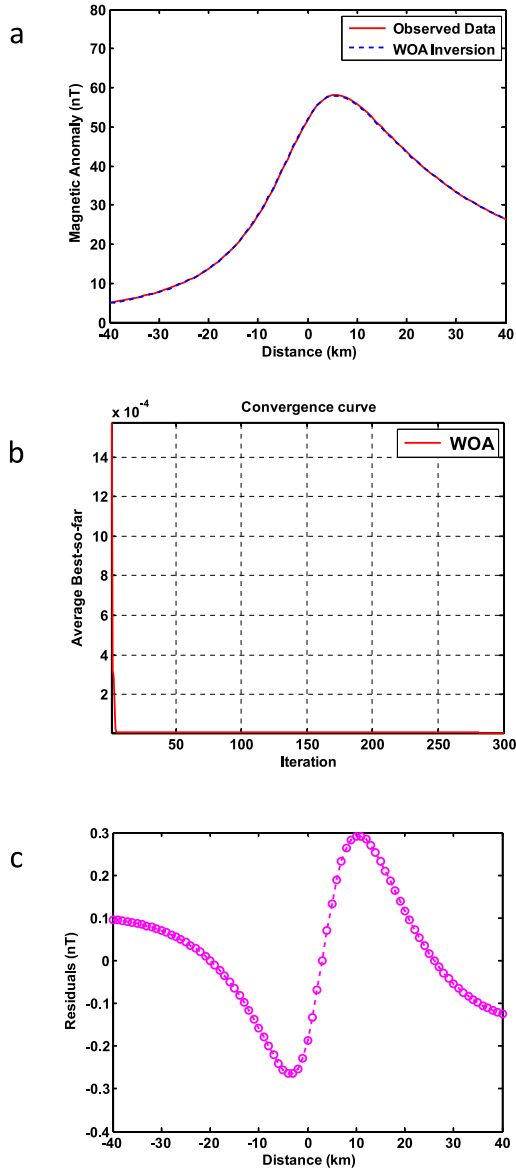


Fig. 9. WOA inversion results for synthetic magnetic anomaly of a noise free 2-D vertical fault model. a) comparison between inverted response (blue) and synthetic data (red), b) convergence curve of the objective function with WOA iterations values, and c) residuals between synthetic magnetic data and inverted magnetic data from WOA.

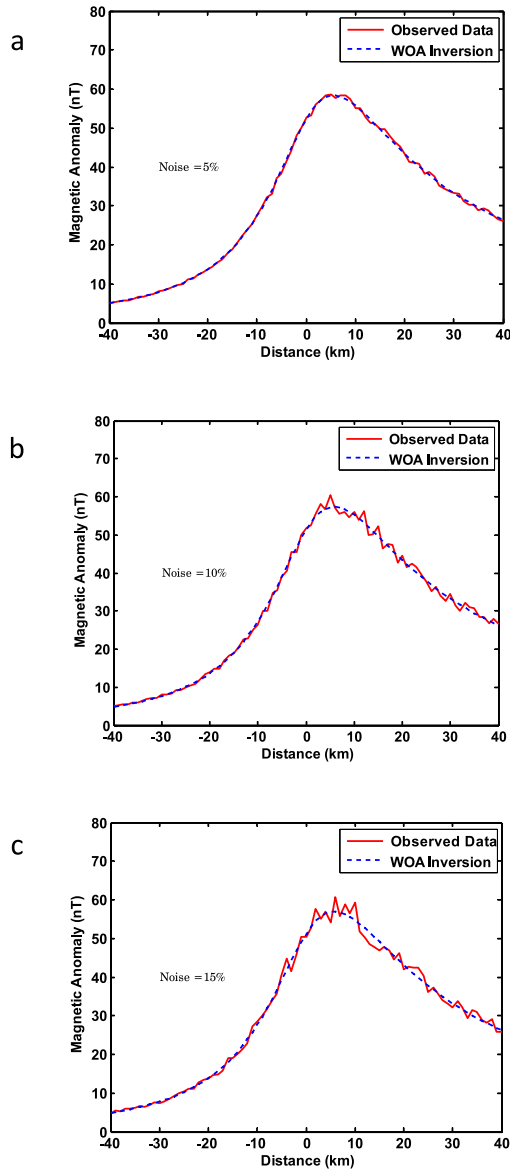


Fig. 10. Synthetic magnetic anomaly of 2-D vertical fault model with their WOA inversion responses for a) with 5% of random noise, b) with 10% of random noise and c) with 15% of random noise.

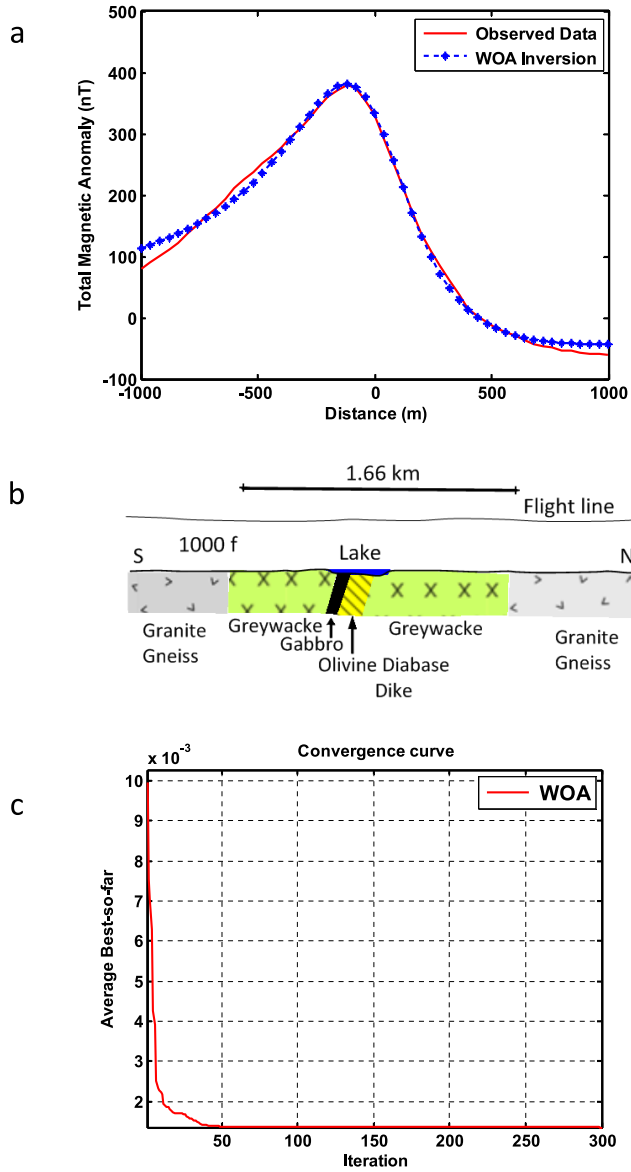


Fig. 11. WOA inversion results for Pishabo Lake magnetic Anomaly (after McGrath and Hood, 1970). a) Predicted response from WOA and measured data (red line), b) the corresponding geological cross-section (after McGrath and Hood, 1970), and c) objective function with iterations.

Table 4. WOA inversion results of Diabase dike, Pishabo Lake, Ontario, Canada (a comparison with other methods). The search spaces for WOA are: 10 : 200000 nT.m (A), $-100 : 100$ m (x_0), $-90 : 90^\circ$ (θ), and 1 : 400 m (h).

Methods	A (nT.m)	x_0 (m)	θ ($^\circ$)	h (m)
<i>El-Araby (2003)</i>	–	–	–	294.00
<i>Ekinci (2016)</i>	141,600.27	–	–37.81	322.55
<i>Al-Garni (2017)</i>	139,736.73	–6.19	–37.37	323.92
WOA	144,200.88	–6.41	–37.14	339.29

4.2. Pima copper mine magnetic anomaly, Arizona, USA

The zone of Pima mining represents one of the greatest porphyry copper mine districts in USA since the nineteenth century. Mineralization interconnected with Laramide igneous activity arises in Paleozoic sedimentary rocks, Mesozoic sedimentary and volcanic sequences, and in Paleocene igneous rocks (*Shafiqullah and Langlois, 1978*). The Pima massive chalcopyrite ore bodies occur between the serpentized dolomitic limestone and the highly altered clay-garnet limestone in an intensely altered zone consisting of a mixture of kaolin and small garnets (Fig. 12a,b), with some limestone remnants (*Thurmond and Storms, 1958*). This alteration suggests the possibility of a nearby intrusive. The thin bedded dolomitic limestone usually forms the foot wall of the massive ore bodies, although in a few places a thin bed of this formation forms the hanging wall. Where the ore body is absent, this thin-bedded, serpentized, dolomitic limestone grades into the highly altered, clay-garnet limestone, with one formation fingering into the other (*Thurmond and Storms, 1958*). Fig. 12c shows a geologic cross section across Pima copper mine.

Fig. 13a shows the vertical magnetic field profile of the Pima copper mine, Arizona, USA (*Gay, 1963*). The profile length of this anomaly is 728 m and a sampling interval of 13 m was used in the digitizing process, so 57 points used in the WOA inversion. The inverted outcomes via WOA are as follows: $A = 41,218.73$ nT.m, $x_0 = -4.24$ m, $h = 67.93$ m, $\theta = -49.19^\circ$. The average best of the misfit function is depicted in Fig. 13b. Differences between observed and computed magnetic data are demonstrated in Fig. 13c. A comparison with other methods (*Gay, 1963; Abdelrahman et al.,*

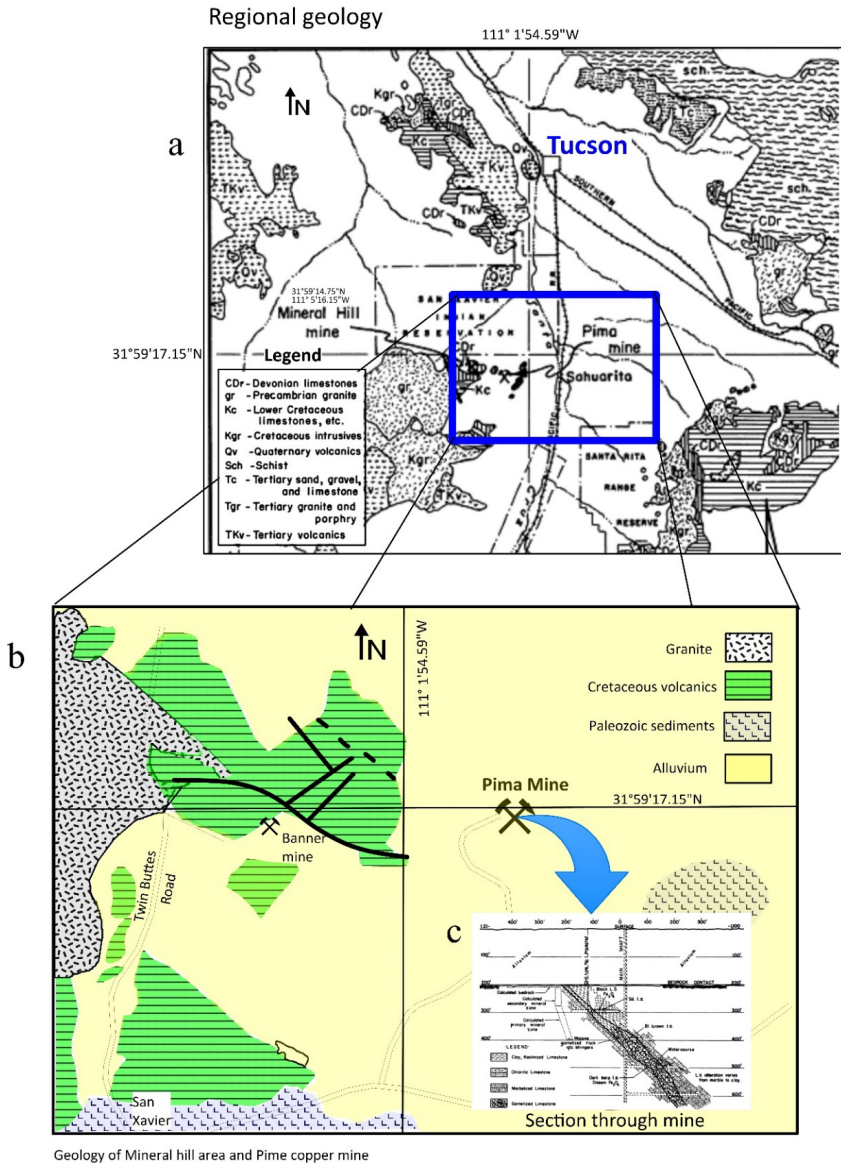


Fig. 12. General Geology of Tucson and surroundings (a), geology of mineral hill area and Pima copper mine (b), and simplified geologic cross section across Pima copper mine (c), (modified after *Thurmond and Storms, 1958*).

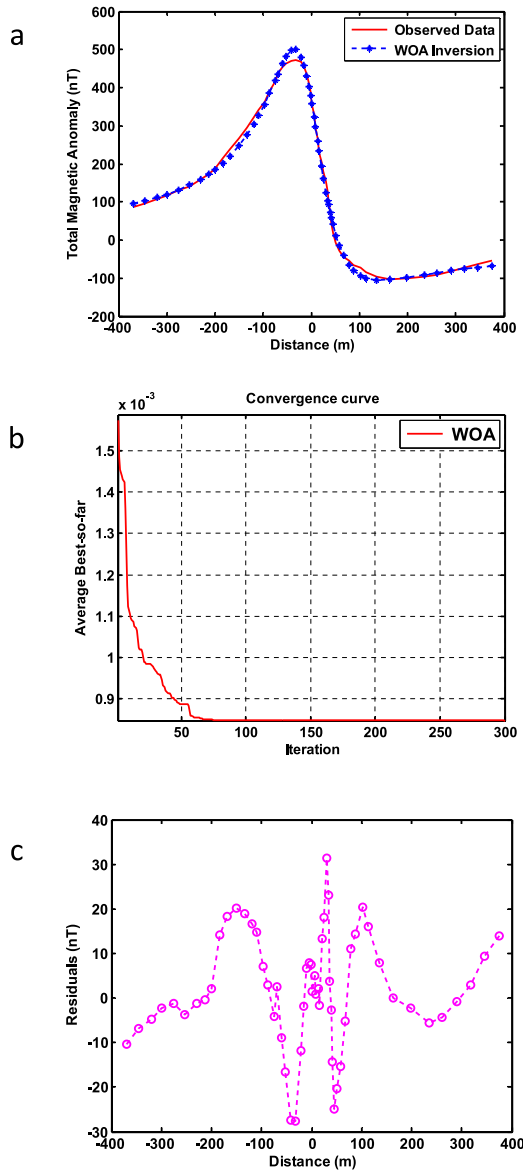


Fig. 13. WOA results for Pima copper mine magnetic Anomaly (after *Gay, 1963*). a) Calculated data from WOA (blue) and measured magnetic data (red), b) cost function with iterations, and c) residuals between measured magnetic response and inverted magnetic response from WOA.

1989; Gobashy, 1999; Asfahani and Tlas, 2007; Tlas and Asfahani, 2011; Ekinici, 2016; Al-Garni, 2017) was shown in Table 5.

Table 5. WOA inversion results of Pima copper mine, Arizona, USA (a comparison with other methods). The search spaces for WOA are: 10 : 100000 nT.m (A_e), -30 : 10 m (x_0), -60 : -40° (θ), and 0 : 100 m (h).

Methods	A_e (nT.m)	x_0 (m)	θ (°)	h (m)
<i>Gay (1963)</i>	–	–	-50	69.80
<i>Abdelrahman and Sharafeldin (1996)</i>	–	–	-53	66.00
<i>Asfahani and Tlas (2007)</i>	–	–	-50.5	71.5
<i>Tlas and Asfahani (2011)</i>	–	-0.22	-47.58	71.25
<i>Ekinici (2016)</i>	39,267.31	–	-50.76	68.29
<i>Al-Garni (2017)</i>	37,065.73	-14.23	-44.78	65.63
WOA	41,218.73	-4.24	-49.19	67.93

4.3. Kiirunavaara iron mine magnetic anomaly, Sweden

Fig. 14a illustrates the vertical component of the magnetic field profile that was measured at the Kiirunavaara iron mine in northern Sweden. This field example is the largest of apatite iron ores in Sweden. *Lynch and Jönberger (2014)* explained that the Kiirunavaara group holds economically very essential iron oxide-apatite ore deposits in the districts of Kiruna and Malmberget. This magnetic field anomaly is resulted from a vein of approximately 20% magnetite (*Grant and West, 1965*). The vertical component magnetic profile has a length of 600 m and a 12 m sampling interval utilized in digitizing of this profile and fifty one points used though the inversion. The retrieved results via WOA are as follows: $A_e = 3,462,694.42$ nT.m, $x_0 = 4.89$ m, $h = 47.07$ m, $\theta = 5.86^\circ$. A comparison with other techniques that interpreted this field example (*Grant and West, 1965; Sundararajan et al., 1985; Ekinici, 2016; Al-Garni, 2017*) was given in Table 6. The WOA results are very similar to those attained from (*Al-Garni, 2017*). The behavior of the cost function is depicted in Fig. 14b. Residuals between observed and computed magnetic data are demonstrated in Fig. 14c.

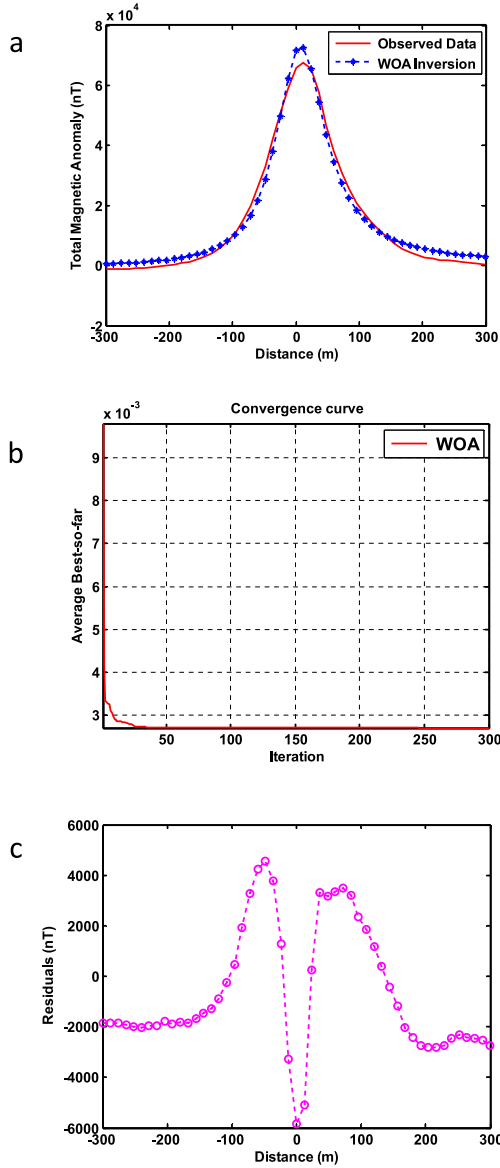


Fig. 14. WOA results for Kiirunavaara iron mine magnetic anomaly (after *Grant and West, 1965*). a) Calculated data from WOA (blue) and measured magnetic data (red), b) cost function with iterations, and c) residuals between measured magnetic response and inverted magnetic response from WOA.

Table 6. WOA inversion results of Kiirunavaara iron mine, Sweden (a comparison with other methods). The search spaces for WOA are: 10 : 10000000 nT.m (A), $-50 : 50$ m (x_0), $-90 : 90^\circ$ (θ), and 1 : 200 m (h).

Methods	A_e (nT.m)	x_0 (m)	θ ($^\circ$)	h (m)
<i>Grant and West (1965)</i>	–	–	–	62–63
<i>Sundararajan et al. (1985)</i>	–	–	–	59.00
<i>Ekinçi (2016)</i>	3,713,125.65	–	10.39	56.09
<i>Al-Garni (2017)</i>	3,483,203.00	13.91	2.17	49.70
WOA	3,462,694.42	4.24	5.86	47.07

4.4. Marcona magnetic anomaly, Marcona district, Peru

The iron oxide-copper-gold (IOCG) mineralization (Mesozoic age) sub-province of littoral south-central Perú, centered at latitude $15^\circ 11'$ S, longitude $75^\circ 6'$ W, incorporates Marcona (Fig. 15a), the pre-eminent central Andean iron oxide deposit (1.9 Gt @ 55.4% Fe), and Mina Justa, one of the few major Andean IOCG deposits with economic copper grades (346.6 Mt @ 0.71% Cu) (*Chen et al., 2010*). The mineralized area is intruded by a swarm of hypabyssal bodies. These range from apparently syn- to clearly post-mineralization and, in composition, from silicic to, rarely, ultramafic (hornblende pyroxenite: *Atchley, 1956*), but magmatic chemistry and mineralogy are almost everywhere disguised by alteration (*Chen et al., 2010*). Fig. 15b shows geology of the Marcona-Mina Justa district (modified from *Chen et al., 2010*). An en echelon array of 12 major magnetite ore bodies (“minas”) and 55 smaller “cuerpos” is recognized in Marcona mine. This is probably the source of the high magnetic anomaly over the mine.

Fig. 16a depicts the magnetic field example due to a dipping dike (*Gay, 1963*) close to the magnetic equator in the Marcona district, Peru which was digitized at 10 m interval and 121 data points is used in the WOA inversion. The inverted parameters by WOA are as follows: $b = 196.44$ m, $I = 1057.78$ nT, $\theta = 58.57^\circ$, $h = 150.00$ m, $\psi = -50.72^\circ$. The misfit error between observed and inverted data from WOA is 0.9824%. Table 7 shows a comparison with other approaches in the literature which studied this field example as a dipping dike (*Gay, 1963; Koulomzine et al., 1970; Pal,*

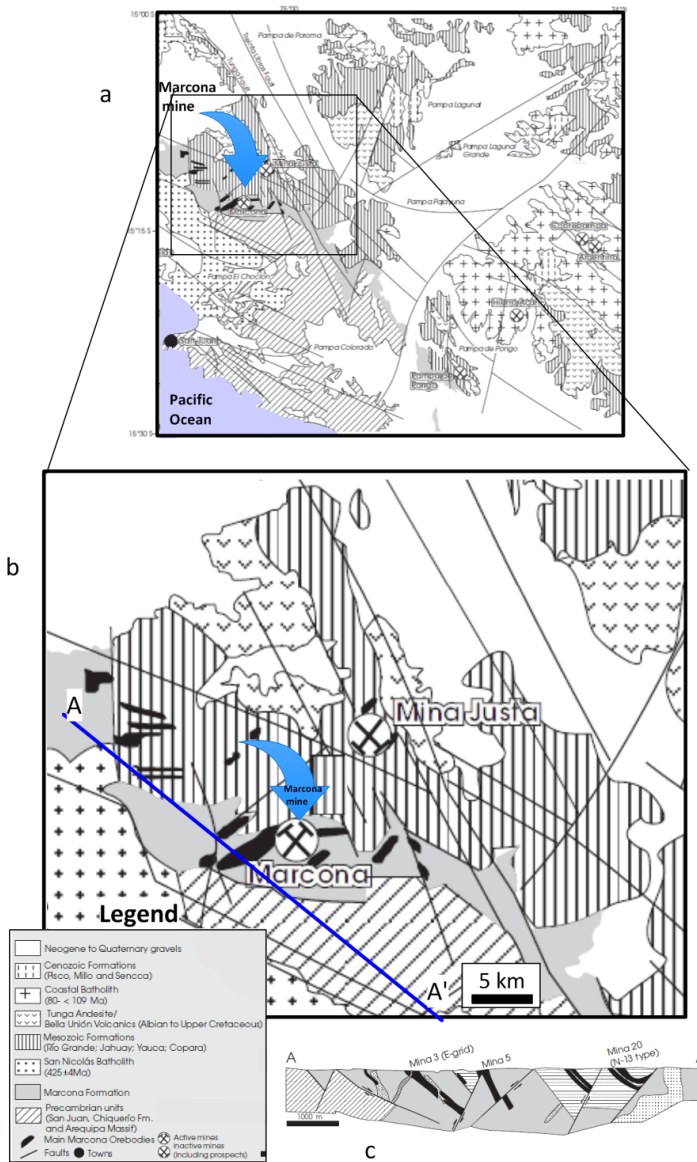


Fig. 15. General geology of the Marcona-Mina Justa district (modified after *Chen et al., 2010*) (a) and (b); Schematic cross section of Marcona mine area (A–A' in Fig. 15a), the magnetite ore bodies are extensively dislocated by faults (c).

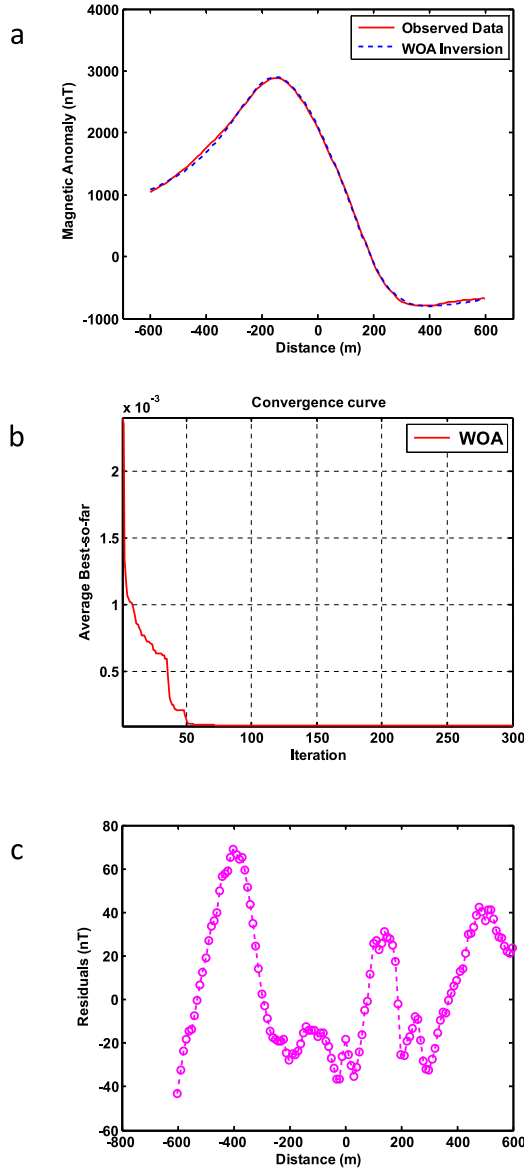


Fig. 16. WOA results for Marcona magnetic Anomaly (after *Gay, 1963*). a) Calculated data from WOA (blue) and measured magnetic data (red), b) cost function with iterations, and c) residuals between measured magnetic response and inverted magnetic response from WOA.

Table 7. WOA inversion results of Marcona magnetic anomaly, Marcona district, Peru (a comparison with other methods). The search spaces for WOA are: 70 : 150 m (h), 100 : 250 m (b), 500 : 1500 nT (I), 10 : 80° (θ), and -80 : 80° (ψ).

Methods	h (m)	b (m)	I (nT)	θ (°)	ψ (°)
<i>Gay (1963)</i>	124.00	186.00	–	–	-50.00
<i>Koulomzine et al. (1970)</i> (1st solution)	126.70	205.95	–	–	-50.10
<i>Koulomzine et al. (1970)</i> (2nd solution)	135.50	202.75	–	–	-50.50
<i>Pal (1985)</i>	132.60	193.75	–	–	-49.30
<i>Al-Garni (2015)</i>	130.00	191.70	808.30	65.49	-64.60
WOA	150.00	196.44	1057.78	58.57	-50.72

1985; Al-Garni, 2015). The inverted outcomes from our algorithm are in well agreement with those attained from methods interpreted this example as in Table 7. The behavior of the objective function is depicted in Fig. 16b and residuals between observed and computed magnetic data are displayed in Fig. 16c.

4.5. The aeromagnetic anomaly of Bihar, India

Fig. 17a depicts the aeromagnetic field anomaly measured at 2500 ft. above a dubitable deep positioned fault southwest of Dehri, Bihar, India. The anomaly is digitized at 1 km interval and 52 data points used in the WOA inversion. The survey area is enveloped by Uindhyan and sediments are connected with Bijawar rocks. The retrieved results via WOA are as follows: $z = 9.235$ km, $x_0 = -2$ km, $z_b = 24.538$ km, $k = 856.400$ nT, $\theta = -131.813^\circ$. Table 8 shows a comparison with other approaches in the literature which studied this field example as a vertical fault (*Qureshi and Nalaye, 1978; Atchuta Rao and Ram Babu, 1983; Asfahani and Tlas, 2007; Tlas and Asfahani, 2011*). The inverted outcomes from our algorithm agreed well with those attained from methods interpreted this example as in Table 8. The average best of the misfit function is depicted in Fig. 17b. Differences between observed and computed magnetic data are demonstrated in Fig. 17c.

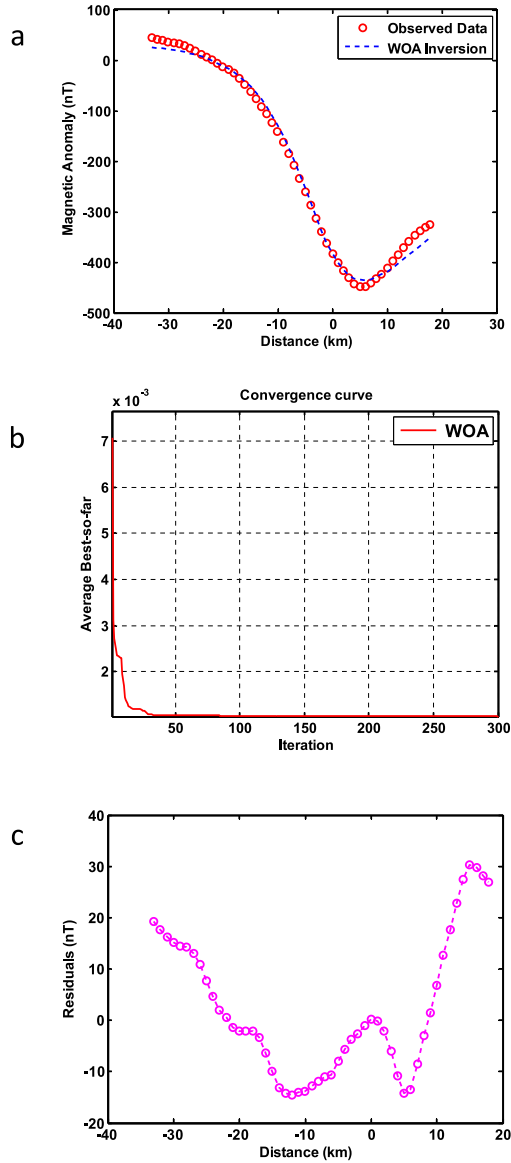


Fig. 17. WOA results for aeromagnetic Field Anomaly of Southwest of Dehri (after *Qureshi and Nalaye, 1978*). a) Calculated data from WOA (blue) and measured magnetic data (red circles), b) cost function with iterations, and c) residuals between measured magnetic response and inverted magnetic response from WOA.

Table 8. WOA inversion results of aero-magnetic of southwest of Dehri anomaly, Bihar, India (a comparison with other methods). The search spaces for WOA are: 1 : 15 km (z), 20 : 50 km (z_b), -4 : 2 km (x_0), -270 : 90° (θ), and 500 : 1000 nT (K).

Methods	z (km)	z_b (km)	x_0 (km)	θ (°)	K (nT)
<i>Qureshi and Nalaye (1978)</i>	7.5	30	–	-133	–
<i>Atchuta Rao and Ram Babu (1983)</i>	8	32	–	-130	–
<i>Asfahani and Tlas (2007)</i>	10.2	25.5	–	-141.7	815
<i>Tlas and Asfahani (2011)</i>	10.54	25.22	0.04	-141.60	789.38
WOA	9.235	24.538	-2	-131.813	856.400

4.6. The magnetic anomaly of the western margin of Perth basin, Australia

The Perth basin is a major rift structure running parallel to the southwestern coast of Australia (Fig. 18). The eastern boundary of the basin is clearly defined by the Darling fault which separates it from the Yilgam block comprising Archaean rocks of the Australian shield (*Qureshi and Nalaye, 1978*). The western boundary of the rift is recognized in the north in the Northampton block and in the south in the Leeuwin block, both made up of Precambrian rocks and faulted on the east to a varying degree of intensity. An aeromagnetic survey conducted by the Bureau of Mineral Resources has revealed that the boundary may underlie the strong anomalies which run roughly in the north-south direction in this region. This magnetic anomaly (*Qureshi and Nalaye, 1978*), is digitized at 1 km interval and 42 data points and used in the WOA inversion (Fig. 19a). The inverted parameters by WOA are as follows: $z = 6.032$ km, $x_0 = -1.731$ km, $z_b = 13.036$ km, $k = 213.161$ nT, $\theta = 48.092^\circ$. The misfit error between observed and inverted data from WOA is 3.7193%. A comparison with other techniques that interpreted this field example (*Qureshi and Nalaye, 1978; Atchuta Rao and Ram Babu, 1983; Asfahani and Tlas, 2007; Tlas and Asfahani, 2011*) was given in Table 9. The behavior of the cost function is depicted in Fig. 19b. Inverted outcomes from our algorithm are in well agreement with those attained from methods interpreted this example as in Table 9. Residuals between observed and computed magnetic data are demonstrated in Fig. 19c.

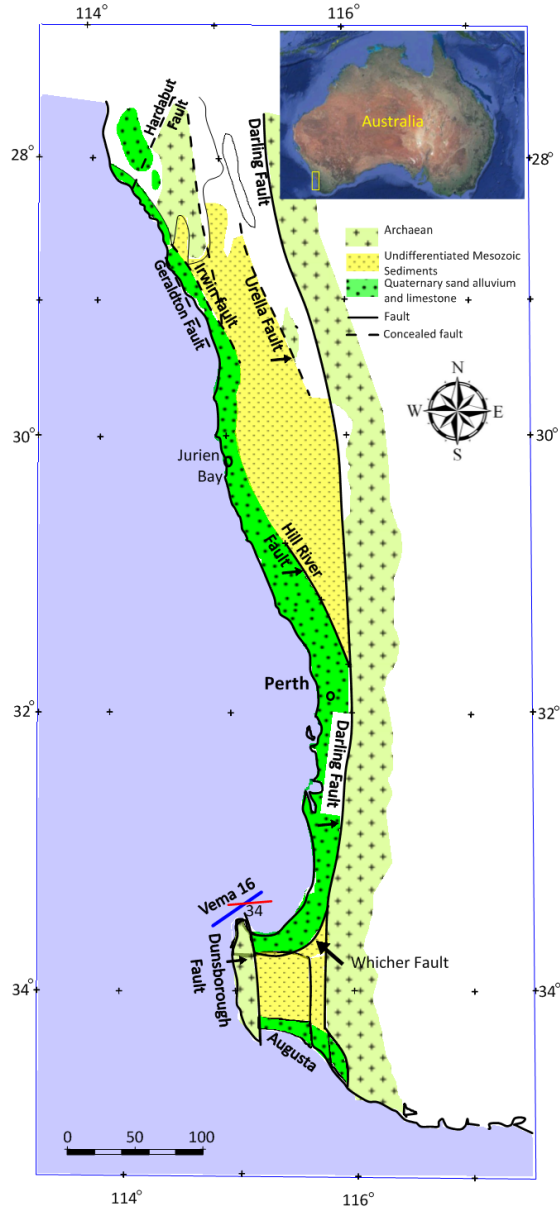


Fig. 18. General geologic map of Perth basin, Australia. Position of faults are posted based on *Wilson (1957)* (figure modified after *Hawkins et al., 1965*).

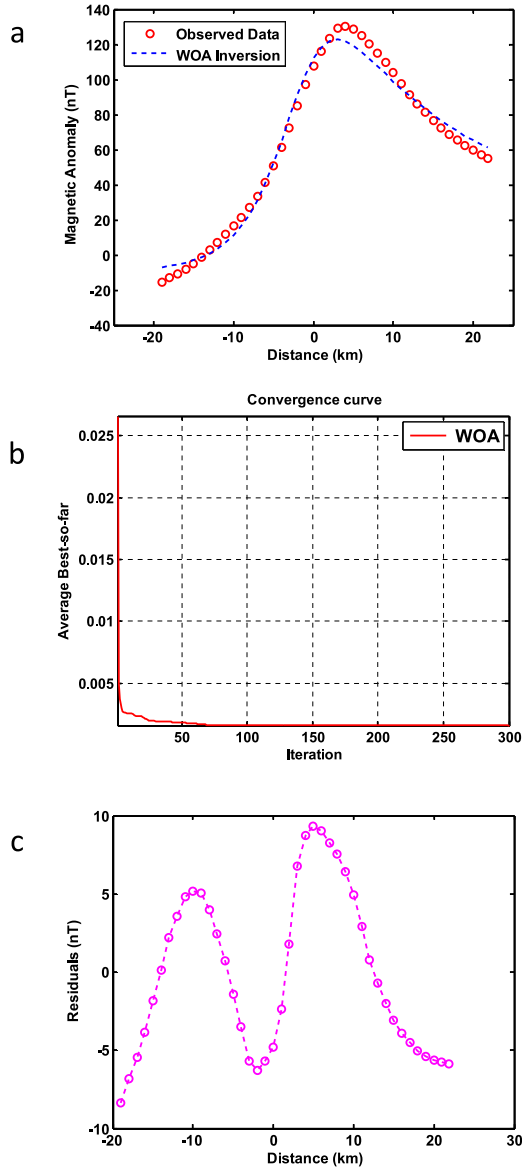


Fig. 19. WOA results for magnetic field anomaly of the western margin of Perth basin (after *Qureshi and Nalaye, 1978*). a) Calculated data from WOA (blue) and measured magnetic data (red circles), b) cost function with iterations, and c) residuals between measured magnetic response and inverted magnetic response from WOA.

Table 9. WOA inversion results of western margin of Perth basin anomaly, Australia (a comparison with other methods). The search spaces for WOA are: 1 : 30km (z), 1 : 100km (z_b), $-4 : 4$ km (x_0), $-90 : 90^\circ$ (θ), and 100 : 300 nT (K).

Methods	z (km)	z_b (km)	x_0 (km)	θ ($^\circ$)	K (nT)
<i>Qureshi and Nalaye (1978)</i>	5.80–6.85	15.55–17.00	–	30	–
<i>Atchuta Rao and Ram Babu (1983)</i>	6.26	15.45	–	40	–
<i>Asfahani and Tlas (2007)</i>	7.5	14	–	39.8	200.3
<i>Tlas and Asfahani (2011)</i>	7.22	13.72	0.88	35.54	200.56
WOA	6.032	13.036	-1.731	48.092	213.161

5. Conclusion

A proficient algorithm is suggested for the elucidation of magnetic field data resulted from simple shaped subsurface geo-bodies like a thin dike, a dipping dike, and a vertical fault using Whale Optimization Algorithm (WOA), global meta-heuristic optimization technique, for ore and mineral investigation. By applying this technique, a best evaluation of the horizontal position, the depth to the upper surface (center) of the buried body, the effective magnetization angle, dip angle of the dipping dike, depths to the upper and to the lower edges of the fault and the amplitude coefficient is easily attained. The efficiency of our algorithm is illustrated through the examination on synthetic magnetic data generated via three different models (thin dike, dipping dike, and vertical fault). Every theoretical model is tested with and without random error, and the highest random error added is 30%.

Being hypothetically proved, this recent suggested algorithm was applied to real case studies from Canada, United States, Sweden, Peru, India, and Australia. The agreement between the results obtained by such a technique and those reported by other interpretation methods is good and comparable. Furthermore, the convergence towards the optimal estimation of parameters is assured and rapidly reached. One more advantage is that the probability of being trapped in local minimum is low, which is an advantage of meta-heuristic methods. Those essential characteristics give the new proposed method power over other published interpretative methods.

References

- Abdelazeem M., Gobashy M., Khalil M. H., Abdrabou, M., 2019: A complete model parameter optimization from self-potential data using Whale algorithm. *J. Appl. Geophys.*, **170**, 103825, doi: 10.1016/j.jappgeo.2019.103825.
- Abdelazeem M., Gobashy M., 2006: Self-potential inversion using genetic algorithm. *Journal of King Abdulaziz University, JKAU: Earth Sci.*, **17**, 1, 83–101, doi: 10.4197/Ear.17-1.5.
- Abdelazeem M., 2001: Robust Numerical Inversion of the magnetic anomalies due to long horizontal cylinders. Paper presented in the second international conference on the geology of Africa, Assiut, Egypt.
- Abdel-Basset M., Manogaran G., El-Shahat D., Mirjalili S., 2018: A hybrid whale optimization algorithm based on local search strategy for the permutation flow shop scheduling problem. *Future Gener. Comput. Syst.*, **85**, 129–145, doi: 10.1016/j.future.2018.03.020.
- Abdelrahman E. M., Bayoumi A. I., Abdelhady Y. E., Gobashy M. M., Elaraby H. M., 1989: Gravity interpretation using correlation factors between successive order least-squares residual anomalies. *Geophysics*, **54**, 12, 1614–1621, doi: 10.1190/1.1442629.
- Abdelrahman E. M., Sharafeldin S. M., 1996. An iterative least-squares approach to depth determination from residual magnetic anomalies due to thin dikes. *J. Appl. Geophys.*, **34**, 3, 213–220, doi: 10.1016/0926-9851(95)00017-8.
- Abdelrahman E. M., Abdelazeem M., Gobashy M., 2019: A minimization approach to depth and shape determination of mineralized zones from potential field data using the Nelder-Mead simplex algorithm. *Ore Geol. Rev.*, **114**, 103123, doi: 10.1016/j.oregeorev.2019.103123.
- Al-Garni M. A., 2015: Interpretation of magnetic anomalies due to dipping dikes using neural network inversion. *Arab. J. Geosci.*, **8**, 10, 8721–8729, doi: 10.1007/s12517-014-1770-7.
- Al-Garni M. A., 2017: Inversion of magnetic anomalies due to isolated thin dike-like sources using artificial neural networks. *Arab. J. Geosci.*, **10**, 15, 337, doi: 10.1007/s12517-017-3115-9.
- Asfahani J., Tlas M., 2007: A robust nonlinear inversion for interpretation of magnetic anomalies caused by faults, thin dikes and spheres like structure using stochastic algorithms. *Pure Appl. Geophys.*, **164**, 2023–2042, doi: 10.1007/s00024-007-0254-z.
- Atchley F. W., 1956: Geology of the Marcona iron deposits, Peru. Unpublished Ph.D. thesis, California, Stanford University, 150 p.
- Atchuta Rao D., Ram Babu H. V., 1983: Standard curves for the interpretation of magnetic anomalies over vertical faults. *Geophys. Res. Bull.*, **21**, 1, 71–89.
- Biswas A., 2015: Interpretation of residual gravity anomaly caused by a simple shaped body using very fast simulated annealing global optimization. *Geosci. Front.*, **6**, 6, 875–893, doi: 10.1016/j.gsf.2015.03.001.

- Biswas A., Acharya T., 2016: A very fast simulated annealing method for inversion of magnetic anomaly over semi-infinite vertical rod-type structure. *Model. Earth Syst. Environ.*, **2**, 4, 198, doi: 10.1007/s40808-016-0256-x.
- Biswas A., Sharma S. P., 2014a: Resolution of multiple sheet-type structures in self-potential measurement. *J. Earth Syst. Sci.*, **123**, 4, 809–825, doi: 10.1007/s12040-014-0432-1.
- Biswas A., Sharma S. P., 2014b: Optimization of self-potential interpretation of 2-D inclined sheet-type structures based on very fast simulated annealing and analysis of ambiguity. *J. Appl. Geophys.*, **105**, 235–247, doi: 10.1016/j.jappgeo.2014.03.023.
- Biswas A., Sharma S. P., 2015: Interpretation of self-potential anomaly over idealized body and analysis of ambiguity using very fast simulated annealing global optimization technique. *Near Surf. Geophys.*, **13**, 2, 179–195, doi: 10.3997/1873-0604.2015005.
- Biswas A., Sharma S. P., 2016: Integrated geophysical studies to elicit the structure associated with Uranium mineralization around South Purulia Shear Zone, India: A review. *Ore Geol. Rev.*, **72**, 2, 1307–1326, doi: 10.1016/j.oregeorev.2014.12.015.
- Bruckshaw J. M., Kunaratnam K., 1963: The interpretation of magnetic anomalies due to dikes. *Geophys. Prospect.*, **11**, 4, 519–522, doi: 10.1111/j.1365-2478.1963.tb02049.x.
- Chen H., Clark A., Kyser T., Ullrich T., Baxter R., Chen Y., Moody T., 2010: Evolution of the Giant Marcona-Mina Justa Iron Oxide-Copper-Gold District, South-Central Peru. *Econ. Geol.*, **105**, 1, 155–185, doi: 10.2113/gsecongeo.105.1.155.
- Ekinici Y. L., 2016: MATLAB-based algorithm to estimate depths of isolated thin dike-like sources using higher-order horizontal derivatives of magnetic anomalies. *Springer Plus*, **5**, 1384, doi: 10.1186/s40064-016-3030-7.
- El-Araby H. M., 2003: Quantitative interpretation of numerical horizontal magnetic gradients over dipping dikes. *Bull. Fac. Sci. Cairo Univ.*, **71**, 97–121.
- El-Kaliouby H. M., Al-Garni M. A., 2009: Inversion of self-potential anomalies caused by 2D inclined sheets using neural networks. *J. Geophys. Eng.*, **6**, 1, 29–34, doi: 10.1088/1742-2132/6/1/003.
- Gay S. P., 1963: Standard curves for interpretation of magnetic anomalies over long tabular bodies. *Geophysics*, **28**, 2, 161–200, doi: 10.1190/1.1439164.
- Gay S. P., 1965: Standard curves for the interpretation of magnetic anomalies over long horizontal cylinders. *Geophysics*, **30**, 5, 818–828, doi: 10.1190/1.1439656.
- Gerovska D., Araúzo-Bravo M. J., 2003: Automatic interpretation of magnetic data based on Euler deconvolution with unprescribed structural index. *Comput. Geosci.*, **29**, 8, 949–960, doi: 10.1016/S0098-3004(03)00101-8.
- Gobashy M. M., 1999: A quasi-Newton scheme for two-dimensional inversion of gravity data. *Delta J. Sci.*, Tanta University, Egypt, **23**.
- Gobashy M., Abdelazeem M., Abdrabou M., Khalil M., 2020: Estimating Model Parameters from Self-Potential Anomaly of 2D Inclined Sheet Using Whale Optimization Algorithm: Applications to Mineral Exploration and Tracing Shear Zones. *Nat. Resour. Res.*, **29**, 1, 499–519, doi: 10.1007/s11053-019-09526-0.

- Göktürkler G., Balkaya Ç., 2012: Inversion of self-potential anomalies caused by simple geometry bodies using global optimization algorithms. *J. Geophys. Eng.*, **9**, 5, 498–507, doi: 10.1088/1742-2132/9/5/498.
- Grant F. S., West G. F., 1965: *Interpretation Theory in Applied Geophysics*. New York: McGraw-Hill, 583 p.
- Hartman R. R., Tesky D. J., Friedberg J. L., 1971: A system for rapid digital aeromagnetic interpretation. *Geophysics*, **36**, 5, 891–918, doi: 10.1190/1.1440223.
- Hawkins L. V., Hennion J. F., Nafe J. E., Thyer R. F., 1965: Geophysical investigations in the area of the Perth Basin, Western Australia. *Geophysics*, **30**, 6, 1026–1052, doi: 10.1190/1.1439686.
- Koulomzine T., Lamontagne Y., Nadeau A., 1970: New methods for the direct interpretation of magnetic anomalies caused by inclined dikes of infinite length. *Geophysics*, **35**, 5, 812–830, doi: 10.1190/1.1440131.
- Ku C. C., Sharp J. A., 1983: Werner deconvolution for automated magnetic interpretation and its refinement using Marquardt's inverse modelling. *Geophysics*, **48**, 6, 754–774, doi: 10.1190/1.1441505.
- Li X., 2003: On the use of different methods for estimating magnetic depth: Lead. *Edge*, **22**, 11, 1090–1099, doi: 10.1190/1.1634912.
- Li X., Yin M., 2012: Application of differential evolution algorithm on self-potential data. *PLoS ONE*, **7**, 12, doi: 10.1371/journal.pone.0051199.
- Lynch E. P., Jönberger J., 2014: Summary report on available geological, geochemical and geophysical information for the Nautanen key area, Norrbotten. Geological Survey of Sweden, report No. 34.
- McGrath P. H., Hood P. J., 1970: The dipping dike case, a computer curve matching method of magnetic interpretation. *Geophysics*, **35**, 5, 831–848, doi: 10.1190/1.1440132.
- Mirjalili S., Lewis A., 2016: The Whale Optimization Algorithm. *Adv. Eng. Softw.*, **95**, 51–67, doi: 10.1016/j.advengsoft.2016.01.008.
- Mohan N. L., Sundararajan N., Seshagiri Rao S. V., 1982: Interpretation of some two-dimensional magnetic bodies using Hilbert transforms. *Geophysics*, **47**, 3, 376–387, doi: 10.1190/1.1441342.
- Monteiro Santos F. A., 2010: Inversion of self-potential of Idealized bodies anomalies using particle swarm optimization. *Comput. Geosci.*, **36**, 9, 1185–1190, doi: 10.1016/j.cageo.2010.01.011.
- Nettleton L. L., 1976: *Gravity and magnetic in oil prospecting*. New York: McGraw-Hill, 464 p.
- Pal P. C., 1985: A gradient analysis based simplified inversion strategy for the magnetic anomaly of an inclined and infinite thick dike. *Geophysics*, **50**, 7, 1179–1182, doi: 10.1190/1.1441992.
- Pasteka R., 2006: The role of the interference polynomial in the Euler deconvolution algorithm. *Boll. di Geofis. Teor. ed Appl.*, **47**, 1-2, 171–180.
- Prakasa Rao T. K. S., Subrahmanyam M., Srikrishna Murthy A., 1986: Nomograms for direct interpretation of magnetic anomalies due to long horizontal cylinders. *Geophysics*, **51**, 11, 2156–2159, doi: 10.1190/1.1442067.

- Qureshi I. R., Nalaye A. M., 1978: A method for the direct interpretation of magnetic anomalies caused by two-dimensional vertical faults. *Geophysics*, **43**, 1, 179–188, doi: 10.1190/1.1440819.
- Reid A. B., Allsop J. M., Granser H., Millet A. J., Somerton I. W., 1990: Magnetic interpretation in three dimensions using Euler deconvolution. *Geophysics*, **55**, 1, 80–91, doi: 10.1190/1.1442774.
- Rao B. S. R., Murthy I. V. R., 1978: Gravity and magnetic methods of prospecting. New Delhi: Arnold Heinneman, 390 p.
- Salem A., 2005: Interpretation of magnetic data using analytic signal derivations. *Geophys. Prospect.*, **53**, 1, 75–82, doi: 10.1111/j.1365-2478.2005.00434.x.
- Salem A., Ravat D., 2003: A combined analytic signal and Euler method (AN-EUL) for automatic interpretation of magnetic data. *Geophysics*, **68**, 6, 1952–1961, doi: 10.1190/1.1635049.
- Shafiqullah M., Langlois J. D., 1978: The Pima mining district Arizona: a geochronologic update. In: Callender J. F., Wilt J., Clemons R. E., James H. L. (Eds.): Land of Cochise (Southeastern Arizona), New Mexico Geological Society 29th Annual Fall Field Conference Guidebook, 348 p., 321–327.
- Sharma S. P., Biswas A., 2013: Interpretation of self-potential anomaly over 2D inclined structure using very fast simulated annealing global optimization – An insight about ambiguity. *Geophysics*, **78**, 3, WB3–WB15, doi: 10.1190/geo2012-0233.1.
- Singh A., Biswas A., 2016: Application of global particle swarm optimization for inversion of residual gravity anomalies over geological bodies with idealized geometries. *Nat. Resour. Res.*, **25**, 3, 297–314, doi: 10.1007/s11053-015-9285-9.
- Sundararajan N., Mohan N. L., Vijaya Raghava M. S., Seshagiri Rao V.S., 1985: Hilbert transform in the interpretation of magnetic anomalies of various components due to thin infinite dike. *Pure Appl. Geophys.*, **123**, 4, 557–566, doi: 10.1007/BF00877453.
- Sungkono S., Desa Warnana D., 2018: Black hole algorithm for determining model parameter in self-potential data. *J. Appl. Geophys.*, **148**, 189–200, doi: 10.1016/j.jappgeo.2017.11.015.
- Sweilam N. M., Abdelazeem M., El-Metwally K., 2007: Self-potential signals inversion to simple polarized bodies using the particle swarm optimization method: A visibility study. *J. Appl. Geophys. (ESAP-Egypt)*, **6**, 1, 195–208.
- Sweilam N. H., Gobashy M. M., Hashem T., 2008: Using particle swarm optimization with function stretching (SPSO) for inverting gravity data: A visibility study. *Journal of Physics and mathematics, Science Bull., Cairo University*, **86**, 2, 259–283.
- Wilson A. F., 1957: Geological map of the older Precambrian rocks of southwest Australia. *J. Roy. Soc. West. Aust.*
- Telford W. M., Geldart L. P., Sheriff R. A., Keys D. A., 1976: Applied Geophysics. Cambridge University Press, Cambridge, 860 p.
- Thurmond R. E., Storms W. R., 1958: Discovery and development of the Pima Copper Deposit, Pima Mining Co., Pima County, Ariz. United States Department of the Interior. Bureau of Mines, information circular 7822.

Tlas M., Asfahani J., 2011: Fair function minimization for interpretation of magnetic anomalies due to thin dykes, spheres and faults. *J. Appl. Geophys.*, **75**, 2, 237–243, doi: 10.1016/j.jappgeo.2011.06.025.